Dyck Triangle in 4D Space

Gennady Eremin

argenns@gmail.com

September 11, 2018

Abstract. In analyzing balanced parentheses, we consider a group of related variables in Dyck paths. In the four-dimensional space, the Dyck triangle is constructed – an integer lattice with Dyck paths.

Key Words: balanced parentheses, diagonal Dyck paths, monotonic lattice paths, double tesseract, Catalan lattice.

Russian version

1 Introduction

In multidimensional spaces (dimension 4 and larger), virtual constructions are usually described, not real objects. Considering balanced parentheses, we found a close relationship of known combinatorial objects. The Dyck triangle with diagonal paths [1], the Dyck triangle with monotonic paths in a square grid [2], and the convolution of the Catalan's matrix [3] are different projections of the same four-dimensional body from the first (positive) hyperoctant.

The above objects are enumerated by Catalan numbers (see A000108), and these numbers are manifested in various problems of discrete mathematics [4]. We have borrowed Figure 1 from Tom Davis [2]. In the left picture we see a diagonal path (or a mountain range) of 12 links located above the zero line. The right picture shows the corresponding monotonic path in a grid of 6 × 6 squares. The monotonic path leads from the lower left corner to the upper right corner, without crossing the main diagonal of the square grid.

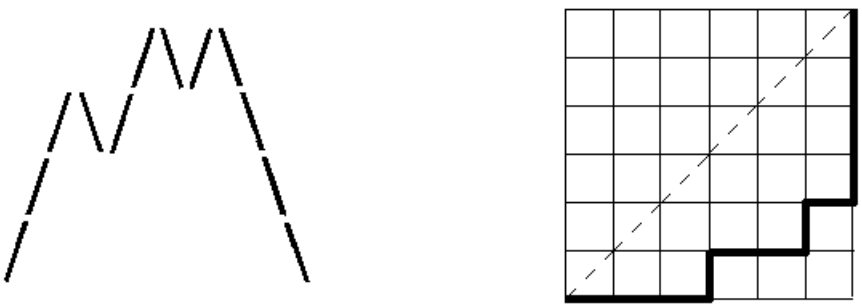

Figure 1: Corresponding Range and Path.

An n-by-n square grid is more interesting because here we see a real triangle (below the diagonal line) with horizontal and vertical links of monotonic Dyck paths of length $2n$ (half-length n). Let's call this object a *Dyck n-triangle* (in our example we have the Dyck 6-triangle).

In Figure 1, both paths are identical, since they correspond to the same balanced parentheses with six open (left) and six closed (right) parentheses

(1) ((( ) (( ) ( )))) .

We liked this definition of balanced parentheses: "a string of parentheses is valid if there are an equal number of open and closed parentheses and if you begin at the left as you move to the right, add 1 each time you pass an open and subtract 1 each time you pass a closed parenthesis, then the sum is always non-negative" [2]. In the bracket group, the left (right) parenthesis corresponds to the upstep (downstep) in the diagonal path and the horizontal (vertical) link in the monotonic path.

The bijection between diagonal paths, monotonous paths and balanced parentheses is obvious. The number of diagonal paths with n upsteps and n downsteps, the number of monotonic paths in a grid of $n \times n$ squares, and the number of balanced parentheses of length $2n$ are equal to the n-th Catalan number. (By the way, what prevents us to consider the balanced parentheses as a kind of Dyck paths?)

In Figure 1, both paths are drawn on a plane in different coordinate grids (the left path contains only diagonal links, in the right picture there are no such links), each grid has its own distinct coordinates. Consequently, the Dyck path can be drawn in three or even four dimensions. There is a natural question, how many types of Dyck paths exist? Obviously, this depends on the number of possible grids and their dimensions.

2 Catalan lattice

2.1. On the plane, we usually draw two (rarely three) coordinate axes, the remaining coordinates for multidimensional objects are represented virtually. Balanced parentheses are convenient because there is direct access to all four coordinates.

Let's return to (1) and start looking at the symbols from left to right, counting the left and right parentheses. Suppose that in some i-th *position* (in our case $i \le 12$) we have counted l *left parentheses* and r *right parentheses*, that is, $i = l + r$. Obviously, $l = r = 6$ for $i = 12$.

In the general case, for the balanced parentheses of length $2n$ in an arbitrary i-th position, we obtain the equality

(2) $$i = l + r,\ \ 2n \geq i \geq l \geq r \geq 0.$$

In addition, often for the balanced parentheses of half-length n, one more variable is introduced, the so-called *unbalance* j. This is the excess of the open (left) parentheses over the closed (right) ones, that is,

(3) $$j = l - r,\ \ n \geq l \geq j \geq 0.$$

Linear equalities (2) and (3) will be called a *coordinate tie*. The variables i and l are dominant, since in the case of zeroing one of them, the others are reset. The variables j and r have a smaller status, and these two variables do not depend on each other. Additionally, note that the sum (or difference) of the variables i and j is even or zero.

The variables i, j, l, r are non-negative integers. Let's call the *Catalan lattice* an infinite set of points in 4D with non-negative integer coordinates (first hyperoctant) that satisfy equalities (1) and (2). Thus in the general case it can be said that the Dyck paths of arbitrary length are located in the Catalan lattice.

In Figure 1 in the two-dimensional version (plane projections), the diagonal Dyck paths are shown in the $i \times j$ grid, and the monotone paths are drawn in the $l \times r$ grid. The reader himself can obtain diagonal-monotonic paths in the $l \times j$ grid (diagonal upsteps and vertical downsteps) and monotonic-diagonal paths in the $r \times j$ grid (vertical upsteps and diagonal downsteps).

The considered two images are modifications of the four-dimensional Dyck triangle. Obviously, there are $\binom{4}{2}$ = 4!/(2!2!) = 6 two-dimensional modifications. The number of 3D modifications is $\binom{4}{3}$ = 4!/(3!1!) = 4. Thus, 11 objects (including a four-dimensional structure) are associated with the Catalan lattice. We will try to get the 4D Dyck triangle, step-by-step starting from objects of smaller dimension.

2.2. We noted that among the 2D projections, the Dyck paths in the $l \times r$ grid are the simplest, most evident, and convenient. On the basis of this modification, we will build Dyck triangles of greater dimension. Let's consider in detail the monotonic path from the previous figure.

Figure 2 shows a 6 × 6 grid with monotonic paths of length 12. The abscissa axis, l-axis, is for left parenthesis; the ordinates axis, r-axis, is for right parenthesis. It is easy to see that in such a modification the Catalan lattice is projected onto an infinite set of nodes bounded by the abscissa axis and the central ray.

The solid line shows the valid links that connect the achievable nodes, forming the Dyck triangle thereby. Invalid links in the grid are dotted; unreachable nodes are omitted. The familiar Dyck path is drawn by a double line.

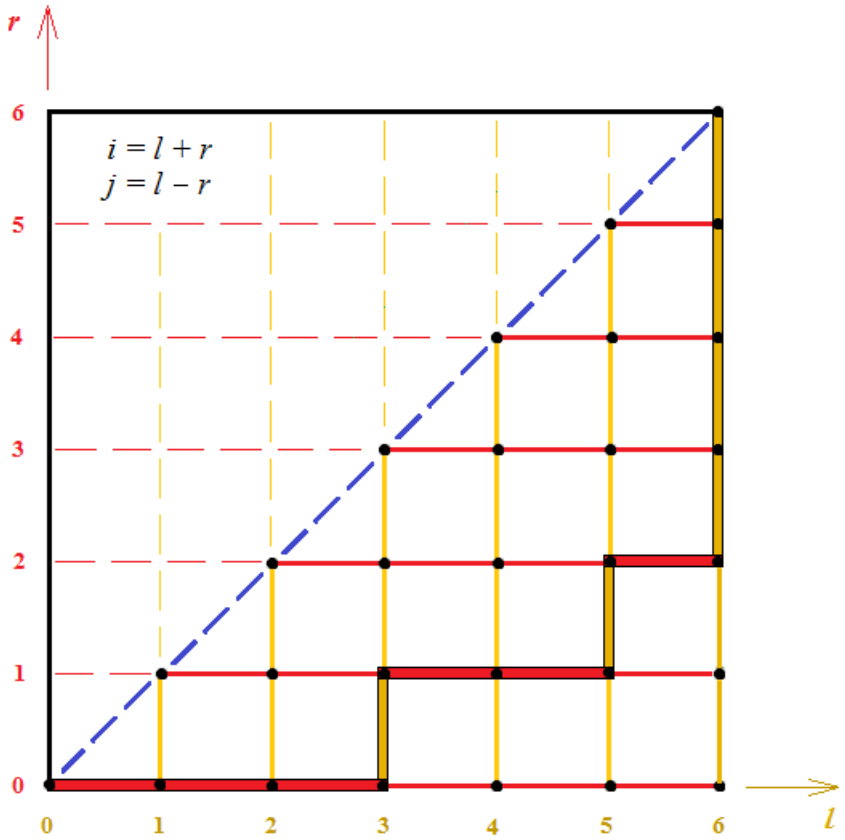

Figure 2: The Dyck triangle in a grid of 6 × 6 squares.

Figure 2 is made using several colors. The yellow color shows everything related to the variable *l*, including *l*-axis and vertical lines, *l-isolines*, which pass through points with the same coordinate *l*. Everything related to the variable *r* is marked in red, including *r*-axis and horizontal *r-isolines*, that connect nodes with the same coordinate *r*. In a blue dotted line, we noted a diagonal line (central ray) that joins nodes for which $j = 0$ ($l = r$).

The abscissa axis is the *r*-isoline number 0 (nodes with zero ordinate). Accordingly, the ordinate axis is the zero *l*-isoline with a single accessible node (0, 0). The central ray is the zero *j*-isoline. Thus, the Dyck 6-triangle is bounded by three isolines: the zero *r*-isoline (the abscissa axis), the 6th *l*-isoline (vertical edge), and the zero *j*-isoline (diagonal).

In Figure 2, the vertices of the Dyck triangle are three points: the origin (0, 0) and the ends of the 6th *l*-isoline, the nodes (6, 0) and (6, 6). Next, we will track the sides and vertices of the Dyck 6-triangle, going over to more complex modifications of the Catalan lattice.

2.3. In a grid of 6 × 6 squares, the number of nodes is $7^2 = 49$, of which $1 + 2 + \ldots + 7 = 28$ are achievable. Obviously, in a grid of $n \times n$ squares, the number of achievable nodes is $1 + 2 + \ldots + (n+1) = (n+1)(n+2)/2$.

We obtain the same number of nodes in all modifications of the 4D Dyck n-triangle. Each achievable node is uniquely determined by an arbitrary pair of coordinates, and this follows from the linear equations (2) and (3). For example, if two coordinates i, j is given, then the other two coordinates in the new grid is defined as follows: $l = (i + j)/2$, $r = (i - j)/2$.

In the introduction we talked about the bijection between different types of Dyck paths of fixed length. In this case we have a *bijection* between nodes of the Dyck n-triangle in different modifications. It is logical to expect that the 4D triangle and its 3D modifications are as flat as the two-dimensional projections. We will check it in the following sections.

3 Grid of $n \times n \times n$ cubes

The square in Figure 2 is converted to a 3D object if we add the i-axis or the j-axis. The range of values for j, l, and r is the same, so the Dyck 6-triangle in the $j \times l \times r$ grid is placed inside the usual $6 \times 6 \times 6$ cube. Since the range for variable i is twice as large, and in the $i \times l \times r$ grid we are dealing with a doubled cube of the size $12 \times 6 \times 6$. We choose the first option, since the usual cube is simple and more convenient.

Figure 3 shows the transition to the $j \times l \times r$ grid. Everything related to the third additional j-axis is shown in blue. The new edges of the formed cube are carried out parallel to the j-axis from the vertices of the original square.

The achievable nodes of the square are labeled by the value of j according to equality (3). The blue color also shows the movement of the square nodes inside the cube, the depth of movement corresponds to the value of the labels. Zero marks the diagonal nodes of the square (zero j-isoline), and these nodes do not move inside the cube under construction.

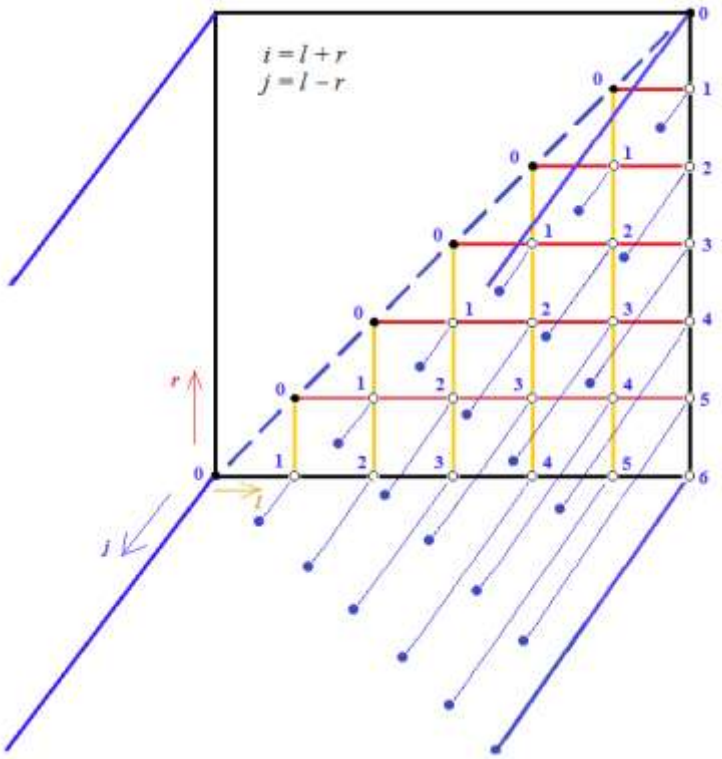

Figure 3: The transition from a 6 × 6 square to a 6 × 6 × 6 cube.

It remains to draw the front face of the cube (parallel to the original square) and also draw *l*-isolines and *r*-isolines inside the cube. In addition, we repeat the previous Dyck path in the cube. The result is shown in Figure 4.

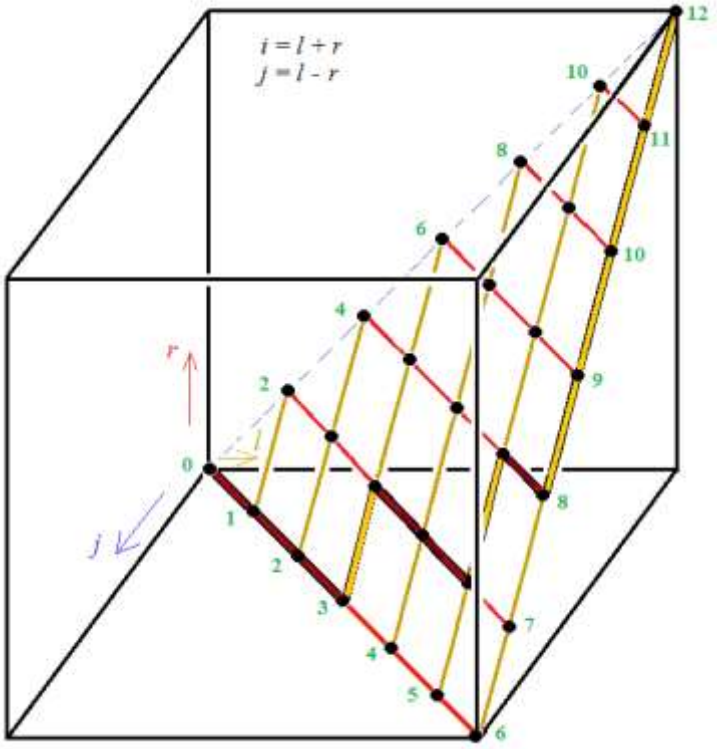

Figure 4: The Dyck 6-triangle in a grid of 6 × 6 × 6 cubes.

When you move from a square to a cube, each edge of the square is converted to a cube face. In this connection, the horizontal and vertical sides of the Dyck 6-triangle (see Figure 3) become diagonals of the cube faces.

In the first octant of the $j \times l \times r$ grid, two diagonals of faces are drawn from the origin (0, 0, 0): a red ray (zero r-isoline) on the jl plane and a blue dotted ray (zero j-isoline) on the lr plane. All points between these two rays form the Catalan lattice in such a 3D projection.

It is easy to see that the Dyck n-triangle is flat inside an $n \times n \times n$ cube. This triangle is cut off in the Catalan lattice by a segment of the nth l-isoline in the face that is parallel to the jr plane. The extreme nodes of the segment are points (n, n, 0) and (0, n, n).

Figure 4 is not very burdened with information, so we additionally marked external nodes of the Dyck 6-triangle with the value of variable i (the sum of $l + r$). Hereinafter, everything connected with the i coordinate is shown in green.

4 Dyck triangle in double tesseract $2n \times n^3$

4.1. The addition of the coordinate axis i perpendicular to the axes j, l, r leads to a 4D space. Among the four-dimensional figures, the most popular is the tesseract (hypercube, tetracube, octagonal) which is obtained if we move the ordinary cube into the fourth dimension by an additional edge and then connect the vertices of both cubes. In our case, the fourth edge is doubled (twice the length), so we are dealing with a four-dimensional parallelepiped in the first hyperoctant (or orthant). Let's call such an object a *double tesseract*.

Figure 5 shows the transition from the 3D cube (the first octant in the $j \times l \times r$ grid) to the double tesseract (the first hyperoctant in the $i \times j \times l \times r$ grid). The direction of the axes is shown at the top left, and the coordinate relationship is repeated. We started the coordinate grid in the far lower node of the original cube. The green color indicates the parts of the picture and the data associated with the fourth dimension.

For a better view, the front top node (0, 6, 6, 6) and the lower right node (0, 0, 6, 0) are not shown in the figure. We showed the movement of achievable nodes of the original cube inside the double tesseract according to the value of i (see Figure 4). It can be seen, only one achievable node, the origin of coordinates, does not move.

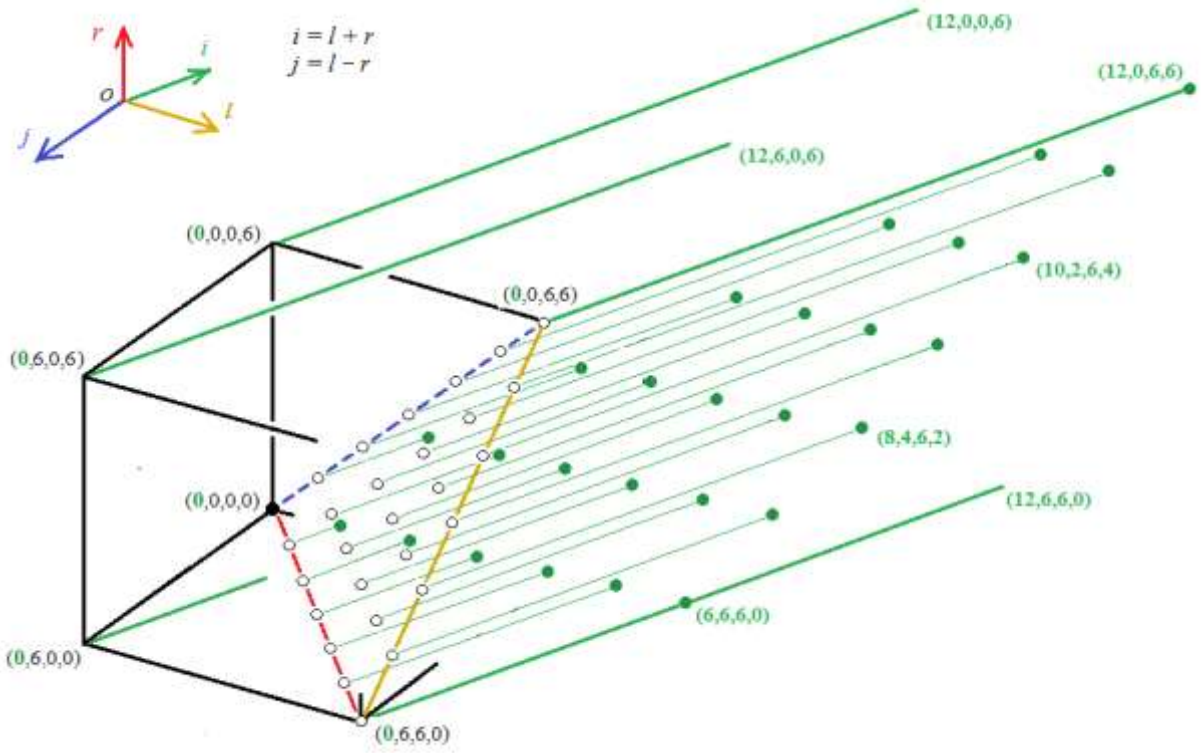

Figure 5: Transition to the 12×6^3 grid.

4.2. In Figure 6, the $i \times j \times l \times r$ grid shows the resulting double tesseract, inside which the 4D Dyck triangle is located (here, familiar Dyck path is repeated). The insides of the triangle are slightly darkened. For a better view, we did not show the front points (0, 6, 6, 6) and (12, 6, 6, 6) in the picture.

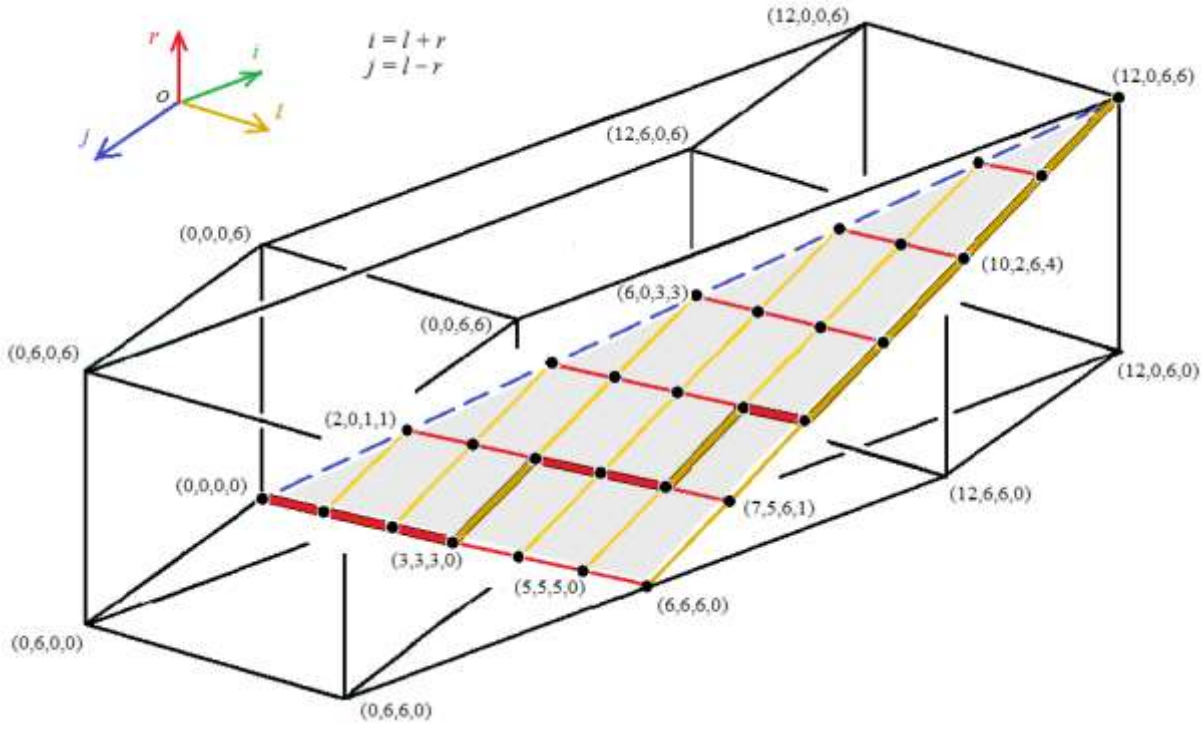

Figure 6: The Dyck 6-triangle in a double tesseract of 12×6^3 4-cubes.

In the double tesseract (as well as in the usual tesseract) there are 16 vertices, 32 edges and 8 three-dimensional faces. Faces are formed by the intersection of a tesseract with eight hyperplanes. In a conventional tesseract, all 3D faces are cubes. In our case, only two faces are 3D cubes, which are clearly visible in Figure 6. The remaining six 3D faces are regular parallelepipeds with two identical dimensions.

4.3. In Figure 6, the four-dimensional Dyck 6-triangle and all its Dyck paths begin at the origin and end at the node (12, 0, 6, 6). Both these nodes and five more accessible nodes form the *blue side* of the Dyck 6-triangle (zero j-isoline, blue dotted line). In addition, we marked the *red side* (zero r-isolines) and the *yellow side* (sixth l-isoline) of the triangle. All three sides are straight lines in this 4D space.

In the general case, the blue side of the Dyck n-triangle is the diagonal of the regular parallelepiped (the 3D face of the double tesseract of size $2n \times n^3$), which contains all nodes with $j = 0$. The parallelepiped is bound by the following nodes

$(0, 0, 0, 0)$, $(0, 0, 0, n)$, $(0, 0, n, n)$, $(0, 0, n, 0)$, $(2n, 0, n, 0)$, $(2n, 0, 0, 0)$, $(2n, 0, 0, n)$, $(2n, 0, n, n)$.

In this list, the origin and the last eighth point are the extreme nodes of the blue side.

The other two sides of the Dyck n-triangle intersect at the point $(n, n, n, 0)$, the center of the edge of the double tesseract with the extreme points $(0, n, n, 0)$ and $(2n, n, n, 0)$. The red side is placed in the regular parallelepiped (another 3D face of the double tesseract), which contains all points with $r = 0$. The parallelepiped is bounded by points

$(0, 0, 0, 0)$, $(0, n, 0, 0)$, $(0, n, n, 0)$, $(0, 0, n, 0)$, $(2n, 0, n, 0)$, $(2n, 0, 0, 0)$, $(2n, n, 0, 0)$, $(2n, n, n, 0)$.

Let us divide this parallelepiped into two equal 3D cubes. Then in the left cube, the red side of the n-triangle becomes a diagonal in the form of a ray with points $(x, x, x, 0)$, $x \le n$.

The yellow side of the Dyck n-triangle is placed in a parallelepiped (another three-dimensional face of a double tesseract), which contains all points of a double tesseract with $l = n$. This parallelepiped is bounded by points

$(0, 0, n, 0)$, $(0, n, n, 0)$, $(0, n, n, n)$, $(0, 0, n, n)$, $(2n, 0, n, n)$, $(2n, 0, n, 0)$, $(2n, n, n, 0)$, $(2n, n, n, n)$.

Divide this parallelepiped into two equal cubes, then in the right cube, the yellow side of Dyck triangle will become the diagonal.

The straightness of the sides of the triangle can be verified by comparing the lengths of the vectors in the 4D space. For example, in the blue side there are six links of the same length $\sqrt{(2^2 + 0^2 + 1^2 + 1^2)} = \sqrt{6}$. On the other hand, the entire length of the blue side is determined by the coordinates of the point (12, 0, 6, 6) and is equal to $\sqrt{(12^2 + 0^2 + 6^2 + 6^2)} = 6\sqrt{6}$.

Also, the red side includes six links with a length of $\sqrt{(1^2 + 1^2 + 1^2 + 0^2)} = \sqrt{3}$. The length of the entire red side is determined by the coordinates of the last vertex (6, 6, 6, 0) and is equal to $\sqrt{(6^2 + 6^2 + 6^2 + 0^2)} = 6\sqrt{3}$. We obtain the same lengths for the yellow side, it follows that the 4D Dyck 6-triangle is not only flat, but also isosceles.

In Figure 2, the red side and yellow side are perpendicular. Let us verify this in 4D space. In the Dyck *n*-triangle, at the intersection of the red side and the yellow side (see Figure 6), we select three points $A(n-1, n-1, n-1, 0)$, $B(n, n, n, 0)$, and $C(n+1, n-1, n, 1)$. For line AB and line BC, the direction vectors are (1, 1, 1, 0) and (1, −1, 0, 1) respectively. It remains to calculate the scalar product of the directing vectors: $1\times1 + 1\times(-1) + 1\times0 + 0\times1 = 0$. This proves the perpendicularity of AB and BC and, respectively, the perpendicularity of the red side and yellow side of the Dyck *n*-triangle.

Conclusion

Thus, the four-dimensional Dyck *n*-triangle is a flat right-angled isosceles triangle. It is interesting that a tie of coordinate variables ensures the independence of modifications. Each modification is self-contained and is able to reincarnate into other modifications (changing coordinate grids) up to the 4D triangle.

We obtained a three-dimensional picture of a double tesseract by moving the ordinary cube to the fourth dimension. But there is another popular projection of a tesseract into 3D space. Figure 7 shows the well-known Schlegel diagram, which is two nested cubes; the neighboring vertices of cubes are connected by straight lines.

In a 4D space, the outer and inner cubes have the same dimensions (of course, this is not the case in the picture). In our case, both cubes are connected by edges of twice the length, and as a result, a double tesseract is formed.

We placed the origin in the lower left node of the outer cube, and the three axes *j*, *l*, and *r* approximates the drawing. The fourth virtual i-axis "leaves" inside both cubes.

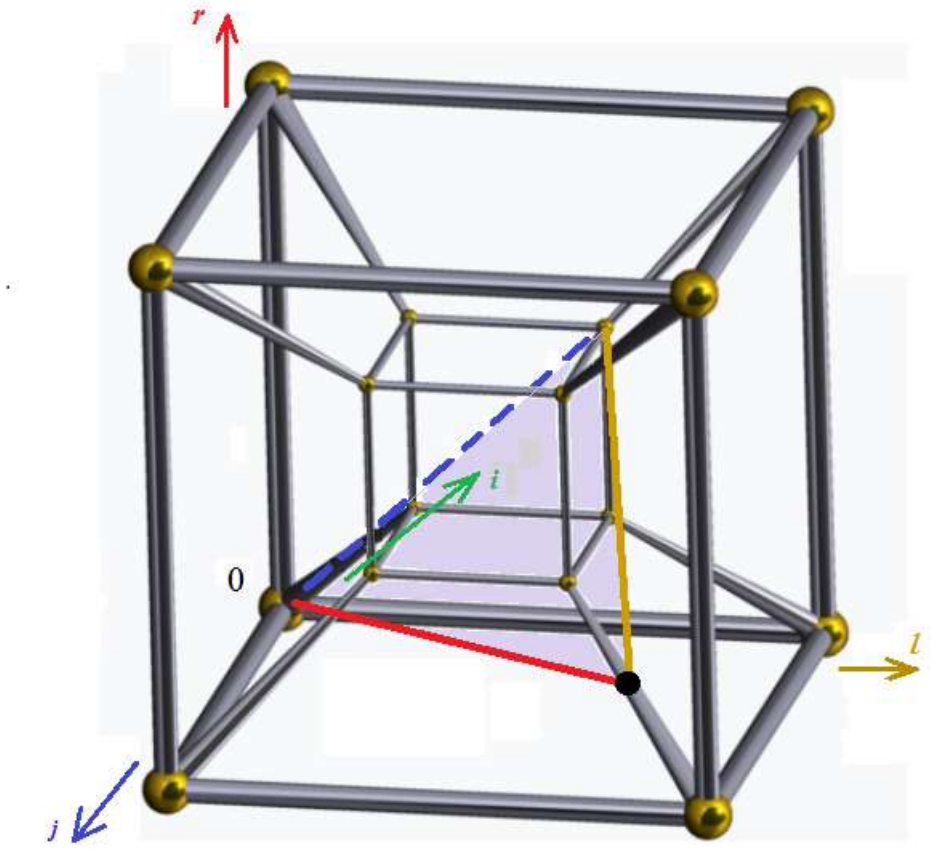

Figure 7: The Dyck *n*-triangle in a Schlegel diagram.

The 4D Dyck *n*-triangle is shown in the diagram by the following three points: (1) the origin, (2) the far right point of the top face of the inner cube, and (3) the center of the doubled edge opposite the origin. We can say that the red and blue sides of the triangle are located on the rays, which limit the Catalan lattice in the 4D space.

References

[1] Lando S. K., *Lectures on Generating Functions*, AMS, 2003. http://www.ams.org/books/stml/023/stml023-endmatter.pdf

[2] Tom Davis, Catalan Numbers, 2015. http://www.geometer.org/mathcircles/catalan.pdf

[3] David Callan, Emeric Deutsch, *The Run Transform*, *Discrete Mathematics*, **312** (2012), 2927-2937. http://www.sciencedirect.com/science/article/pii/S0012365X12002233

[4] R. P. Stanley, *Catalan Numbers*, Cambridge University Press, 2015. http://www.cambridge.org/ro/academic/subjects/mathematics/discrete-mathematics-information-theory-and-coding/catalan-numbers?format=HB